APPLIED PHYSICS LETTERS **102**, 042110 (2013)

Schottky barrier height extraction from forward current-voltage characteristics of non-ideal diodes with high series resistance

Khaled Ahmed and Tony Chiang
Intermolecular, Inc., 3011 N First Street, San Jose, California 95134, USA

(Received 26 December 2012; accepted 17 January 2013; published online 1 February 2013)

Forward bias current-voltage (*I-V*) characteristics measured at room temperature were used to extract Schottky barrier heights in sulfur-implanted PtSi/*n*-Si and NiGe/*n*-Ge contacts. It is found that *I-V* data claimed to support barrier height reductions of ~700 meV and ~500 meV are more consistent with ~300 meV and 100 meV reductions, respectively. These estimates should better guide attempts aiming at finding physical models for the observed reductions. © *2013 American Institute of Physics*. [http://dx.doi.org/10.1063/1.4789989]

Alternative contact architectures are now being sought to improve the interface contact resistance to *n*-Si (for silicon channel CMOS) and to *n*-SiGe or *n*-Ge (for germanium channel CMOS) by reducing the Schottky barrier height (SBH) between metal and *n*-type *S*/*D* semiconductors.[1] Sulfur implantation prior to silicide[2] or germanide[3] formation has been reported to reduce the electron Schottky barrier height to ~0.1 eV. Recently, Connelly and Clifton[4] pointed out that data claimed to support a barrier height between Cl-implanted NiSi and Si of as low as 0.08 V were consistent with much higher barrier heights when the effects of series resistance (R_S) and junction non-ideality (n) are considered. Inspired by Connelly's work, we analyze published *I-V* curves obtained on PtSi/*n*-Si[2] and NiGe/*n*-Ge[3] contacts where sulfur was implanted in the semiconductor prior to PtSi or NiGe formations. We report very different estimates for the barrier height reductions and discuss the technological implications of these estimates.

Current transport in metal/semiconductor diodes is determined by the value of a characteristic energy defined as[5]

$$E_{00} = (qh/\pi)\sqrt{N_D/(4\varepsilon m^*)}. \tag{1}$$

For *n*-Si at room temperature, when $E_{00} \leq 0.2\ kT$ (i.e., $N_D \leq 2\times 10^{17}\ \mathrm{cm}^{-3}$), thermionic-emission current (J_{TE}) dominates carrier transport. When $0.5\ kT \leq E_{00} \geq 2\ kT$ (i.e., $10^{18} \leq N_D \leq 2\times 10^{19}\ \mathrm{cm}^{-3}$), thermionic-field-emission current (J_{TFE}) dominates carrier transport. When $E_{00} \geq 5\ kT$ (i.e., $N_D \geq 1\times 10^{20}\ \mathrm{cm}^{-3}$), field emission current (J_{FE}) dominates carrier transport.

For $V > 3kT/q$, the expression for the *I-V* characteristic is given by

$$I \approx I_0 \exp\left(\frac{V - IR_S}{n\dfrac{kT}{q}}\right), \tag{2}$$

with

$$I_0 \approx a\ A^{**}T^2\exp(-\varphi_{B,eff}/kT) \tag{3}$$

in the thermionic emission conduction regime.[5,6]

The form of the current dependence on voltage given by Eq. (2) is also valid for thermionic-field-emission and field-emission conduction regimes.[6–8]

In the thermionic-field-emission conduction regime, I_0 and n may be expressed as[8]

$$I_{0,TFE} \approx a\ A^{**}\frac{\sqrt{\pi E_{00}(\phi_{B,eff} - V - \xi)}}{kT\cosh\left(\dfrac{E_{00}}{kT}\right)}e^{\left(\frac{\xi}{kT} - \frac{\phi_{B,eff}+\xi}{E_0}\right)}, \tag{4a}$$

$$n_{TFE} \approx \frac{E_{00}}{kT}\coth\left(\frac{E_{00}}{kT}\right). \tag{4b}$$

And in the field-emission conduction regime, I_0 and n may be expressed as[8]

$$I_{0,FE} \approx a\ A^{**}\frac{e^{-\frac{\Phi_{B,eff}}{E_{00}}}}{(c_1 kT)^2}\frac{\pi c_1 kT}{\sin(\pi c_1 kT)}, \tag{5a}$$

$$n_{FE} \approx \frac{E_{00}}{kT}. \tag{5b}$$

In the above equations, c_1, E_0, and ξ are given by[8]

$$c_1 = \frac{ln\left(\frac{4(\phi_{B,eff} - V)}{\xi}\right)}{2E_{00}}, \tag{6a}$$

$$E_0 = E_{00}\coth\left(\frac{E_{00}}{kT}\right), \tag{6b}$$

$$\xi = E_F - E_C. \tag{6c}$$

The parameters used in Eqs. (1)–(6) are defined in Table I.

As can be seen from the above set of equations, the voltage dependence of the current takes the same form (Eq. (2)) but the I_0 and n have different dependence on the diode Schottky barrier height and semiconductor doping density. If I_0 can be extracted from *I-V* curves of diodes fabricated on lightly doped semiconductor, one may extract an effective barrier height based on Eq. (3). The accuracy of the extraction of I_0 determines the accuracy of extracted $\phi_{B,eff}$.

The extraction of the barrier-height from a single *I-V* curve measured at room temperature has been proposed and used in many works in the past.[9–14] In this work, a Levenberg-Marquart curve-fitting algorithm[15] is used for the extraction of transport model parameters from a single *I-V*

TABLE I. Model parameters definitions.

Variable	Definition	Units
V	Metal-to-semiconductor bias voltage	V
$\phi_{B,eff}$	Effective barrier height when *I-V* curve is fitted to thermionic emission [Eq. (3)]	eV
a	Diode area	m^2
T	Temperature	K
R_S	Parasitic series resistance	Ω
ε	Semiconductor dielectric constant	F/m^2
n	Diode ideality factor	–
A^{**}	Effective Richardson's constant	$A/K^2\ m^2$
m^*	Electron tunneling effective mass	kg
N_D	Semiconductor doping density	m^{-3}
k	Boltzmann's constant (1.380×10^{-23})	$m^2\ kg\ s^{-2}\ K^{-1}$

curve measured at room temperature. Curve fitting of experimental data to Eq. (2) is done over the bias range $3kT \leq qV \leq \phi_B - (E_g/2 - \varphi_F)$, where E_g is the semiconductor band gap and φ_F is the Fermi level position with respect to mid-gap. The results of the fit are I_0, R_S, and n. From I_0, $\phi_{B,eff}$ is accurately determined according to Eq. (3). A^{**} for n-Si is $110\,A/K^2\ cm^2$ and for n-Ge is $140\,A/K^2\ cm^2$. This methodology avoids inconveniences and uncertainties associated with graphical techniques.[9–12] In order to ensure that the obtained set of parameters is unique, the following have been performed: (1) Checking the residual to make sure that there is no correlation with V or I when the *I-V* curve is fitted to the model of Eq. (2). (2) Checking the distribution of the residuals using the *Q-Q* plot and making sure it is linear. (3) Elimination of influence points by performing 1000 *Bootstrapping* trials on randomly selected subset *I-V* curves from the original *I-V* curve.[16] (4) Studying the dependence of extracted parameters on the initial values of the fitting parameters. No detectable dependence was found for all data analyzed in this work. (5) Evaluating the statistical significance of the fit using χ^2. We found that χ^2 is always statistically significant.

Current-voltage curves published in Ref. 2 for PtSi/n-Si are shown in Fig. 1 over the bias range $3kT \leq qV \leq \phi_B - (E_g/2 - \varphi_F)$ along with best fit to Eq. (2). Excellent fit was obtained for curves corresponding to different sulfur implant doses. The extracted $\phi_{B,eff}$ is shown in Fig. 2 as function of sulfur implant dose. The extractions done in this work (considering both R_S and n) is very different from those reported in Ref. 2 for non-zero sulfur implant doses. The methods agree for the data without sulfur implant, however, testifying that the extraction methodology is valid and that the curve fitting algorithm used here results in a unique set of parameters: I_0, n and R_S for a given *I-V* curve. The reason for discrepancy for non-zero sulfur implant dose is that the voltage drop across R_S becomes more significant when the current is enhanced for samples with non-zero sulfur implant dose and, if not corrected for, R_S effect will lead to significant under-estimation of $\phi_{B,eff}$. The difference in extracted effective barrier height due to R_S and n was also observed by Connelly and Clifton on a different contact system.[4]

Current-voltage curves published[3] for NiGe/n-Ge were fitted to Eq. (2) over the bias range $3kT \leq qV \leq \phi_B - (E_g/2 - \varphi_F)$. Excellent fit between data and model was obtained for curves with and without sulfur implantation. The effective barrier heights extracted from this data are shown in Fig. 3. The first observation is that the extracted $\phi_{B,eff}$ without sulfur implant agrees with the previous extraction.[3] However, the extracted $\phi_{B,eff}$ from the *I-V* curve corresponding to sulfur-implanted contact shows a large discrepancy. This is similar to the result on PtSi/n-Si contacts presented in the previous paragraph of this letter.

In summary, when properly accounting for R_S and n, $\phi_{B,eff}$ was found to decrease with sulfur implantation but not as much as previously reported.[2,3] The reduction in $\phi_{B,eff}$ from the case without sulfur implant is ~100 meV for NiGe/n-Ge system (compared to ~500 meV reported in Ref. 3), and ~300 meV for PtSi/n-Si system (compared to ~700 meV reported in Ref. 2). The observed reduction in $\phi_{B,eff}$ is still considerable. In Ref. 2, $\phi_{B,eff}$ was extracted using measured current under low forward bias voltage. In Ref. 3, $\phi_{B,eff}$ was extracted from measured reverse biased current dependence on temperature based on Eq. (3) (i.e., assuming thermionic emission conduction). The reverse current in Refs. 2 and 3 is much higher than what the thermionic emission theory predicts from

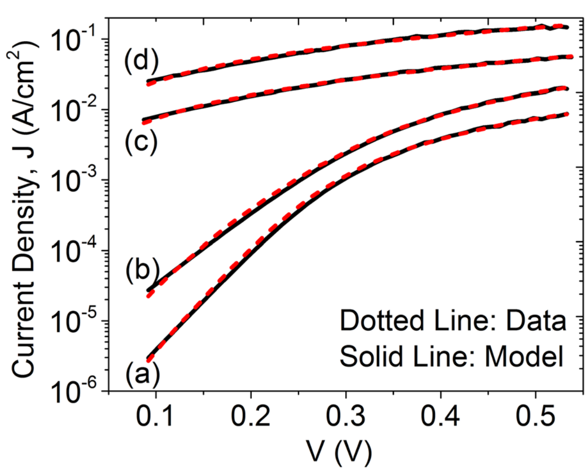

FIG. 1. Experimental data and best model fit (Eq. (2)) for samples with different sulfur implant doses: (a) 0.0, (b) $10^{13}\,cm^{-2}$, (c) $5 \times 10^{13}\,cm^{-2}$, and (d) $10 \times 10^{13}\,cm^{-2}$. Data taken after Alptekin *et al.*[2]

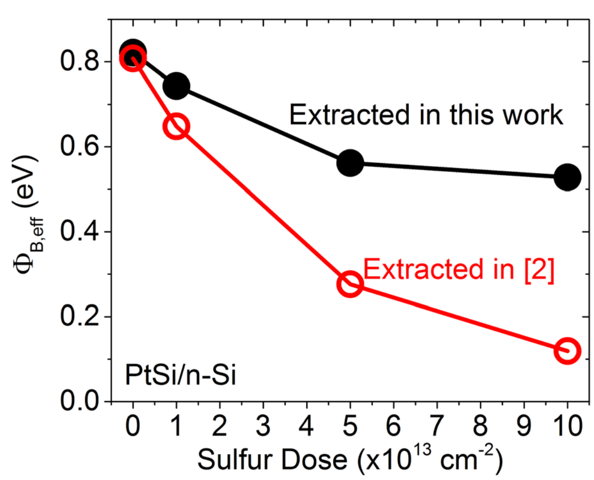

FIG. 2. Extracted Schottky barrier height versus sulfur dose in PtSi/n-Si contacts. Extracted values in this work consider both series resistance and junction non-ideality. Both extractions were done on the same the *I-V* data published in Ref. 2.

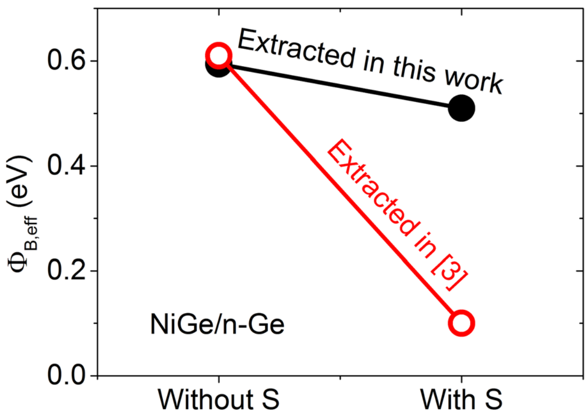

FIG. 3. Extracted Schottky barrier height with and without sulfur implantation prior to NiGe formation. Data taken after Tong *et al.*[3]

fitting forward bias *I-V* curves done in this work. This could be explained by inhomogeneous barrier height as suggested in Refs. 17 and 18 on different contact systems.

[1]Z. Zhang, F. Pagette, C. D'Emic, B. Yang, C. Lavoie, Y. Zhu, M. Hopstaken, S. Maurer, C. Murray, M. Guillorn, D. Klaus, J. Bucchignano, J. Bruley, J. Ott, A. Pyzyna, J. Newbury, W. Song, V. Chhabra, G. Zuo, K.-L. Lee, A. Ozcan, J. Silverman, Q. Ouyang, D.-G. Park, W. Haensch, and P. M. Solomon, IEEE Electron Device Lett. **31**(7), 731 (2010).

[2]E. Alptekin, M. C. Ozturk, and V. Misra, IEEE Electron Device Lett. **30**(4), 331 (2009).

[3]Y. Tong, B. Liu, P. S. Y. Lim, and Y.-C. Yeo, IEEE Electron Device Lett. **33**(6), 773–775 (2012).

[4]D. Connelly and P. Clifton, IEEE Electron Device Lett. **31**(5), 417–418 (2010).

[5]S. M. Sze, *Physics of Semiconductor Devices* (John Wiley & Sons Inc., 1981).

[6]E. H. Rhoderick and R. H. Williams, *Metal-Semiconductor Contacts* (Clarendon, Oxford, 1988).

[7]M. K. Hudait and S. B. Krupanidhi, Physica B **307**, 125–137 (2001).

[8]F. Padovani and R. Stratton, Solid-State Electron. **9**, 695–707 (1966).

[9]S. K. Cheung and N. W. Cheung, Appl. Phys. Lett. **49**(2), 85 (1986).

[10]V. Aubry and F. Meyer, J. Appl. Phys. **76**(12), 7973 (1994).

[11]F. J. Garcia Sanchez, A. Ortiz-Conde, and J. J. Liou, IEE Proc. Circuits Devices Syst. **143**(1), 68 (1996).

[12]T. C. Lee, S. Fung, C. D. Beling, and H. L. Au, J. Appl. Phys. **72**, 4739 (1992).

[13]K. Wang and M. Ye, Solid-State Electron. **53**, 234–240 (2009).

[14]A. Ferhat-Hamida, Z. Ouennoughi, A. Hoffmann, and R. Weiss, Solid-State Electron. **46**, 615–619 (2002).

[15]H. M. Antia, *Numerical Methods for Scientists and Engineers* (Hindustan Book Agency, 2002).

[16]D. MacSweeney, K. G. McCarthy, L. Floyd, M. Riordan, L. Sattler, A. Mathewson, J. A. Power, and S. C. Kelly, in *Proceedings of the International Conference on Microelectronic Test Structures* (2001), pp. 47–52.

[17]V. Janardhanam, Y.-K. Park, H.-J. Yun, K.-S. Ahn, and C.-J. Choi, IEEE Electron Device Lett. **33**(7), 949 (2012).

[18]M. Bhatnagar, B. Jayant Baliga, H. R. Kirk, and G. A. Rozgonyi, IEEE Trans. Electron Devices **43**(1), 150 (1996).